TITLE: Expanding antimicrobial chemical space by engineering drug safety

AUTHORS: Tahoura Samad[1,7], Chayanon Ngambenjawong[1,5], Henry Ko[1], Savan Patel[6], Cristiana DeAgazio[1], Heather E. Fleming[1,2,8], Sangeeta N. Bhatia[1,2,4,6,7,8]

AFFILIATIONS:

1. Koch Institute for Integrative Cancer Research, Massachusetts Institute of Technology, Cambridge, MA 02139
2. Marble Center for Cancer Nanomedicine, Massachusetts Institute of Technology, Cambridge, MA 02139
3. Department of Biology, Massachusetts Institute of Technology, Cambridge, MA 02139
4. Department of Electrical Engineering and Computer Science, Massachusetts Institute of Technology, Cambridge, MA 02139
5. School of Biomolecular Science and Engineering, Vidyasirimedhi Institute of Science and Technology (VISTEC), Rayong, Thailand
6. Harvard-MIT Division of Health Sciences and Technology, Cambridge, MA 02139
7. Institute of Medical Engineering and Science, Massachusetts Institute of Technology, Cambridge, MA 02139
8. Howard Hughes Medical Institute, Massachusetts Institute of Technology, Cambridge, MA 02139

ABSTRACT:

Antibiotic-resistant (AMR) bacterial infections are a major global health threat. Despite the critical need for new antimicrobials, progress is constrained by protracted development timelines, as well as the requirement for chemical novelty to avoid cross-resistance. Although advances in high-throughput screening, genome mining, and machine learning have greatly accelerated antimicrobial discovery, insufficient separation between antibacterial efficacy and host toxicity remains a bottleneck, precluding the clinical development of many promising compounds. Here, we establish a generalizable, two-component strategy to engineer antimicrobial safety and mobilize otherwise inaccessible chemical space for antimicrobial therapy, using calicheamicin, a potent cytotoxin with unacceptable host toxicity, as a proof of concept. In the first arm, we engineer a conditionally-active drug conjugate that limits calicheamicin activity to infected tissue, thereby reducing systemic toxicity. In the second arm, we co-

administer a re-engineered self-resistance enzyme from *Micromonospora echinospora*, the natural producer of calicheamicin, as an “antidote” to neutralize calicheamicin present outside of infected tissue, further mitigating off-target toxicity. The conditionally-active conjugate exhibits activity against Gram-negative and Gram-positive pathogens in response to a protease present within the infected microenvironment. When delivered in combination with the antidote, antibacterial efficacy is maintained while off-target toxicity is reduced in mouse models of Gram positive and negative bacterial pneumonia. We anticipate that our dual strategy, which engineers, rather than selects for enhanced drug safety, by combining conditional drug activity with antidote-driven neutralization of off-target effects, provides a generalizable framework for mobilizing other promising but toxic compounds as antimicrobials.

INTRODUCTION:

Antimicrobial-resistant (AMR) infections are a critical health threat. The World Health Organization (WHO) estimates that resistance to existing drugs directly caused 1.27 million deaths globally and contributed to an additional 4.95 million deaths in 2019 (*1*). Development of new agents to address AMR infections is slow, hindered by the lengthy and costly processes of drug discovery and regulatory approval (*2*), and further challenged by cross-resistance, in which newly developed compounds that are similar to existing antibiotics are subject to the rapid development of resistance (*3*). Additionally, the economics of antibiotic treatment, which can involve short courses of treatment and stewardship programs to limit use, disincentivize investment in antimicrobial development by industry (*2*). Together, these scientific, regulatory, and economic hurdles have resulted in a widening gap between the rise of AMR and the pace of antibiotic development. Given this landscape, there is a critical need for innovative approaches to create antibiotics rapidly, while introducing compounds with novel chemical structures or mechanisms of action that help insulate against cross-resistance.

Recent advances in antibiotic discovery have dramatically expanded our ability to identify compounds with antimicrobial activity. High-throughput screening of small molecule and natural product libraries, machine learning-guided discovery and generation (4-7), large-scale chemical-genetic profiling (8), computational modeling of compound-target interactions (9), and genome mining approaches (10, 11)

55 have increased both the speed and scale of discovery. However, despite this growing discovery capacity,
56 there remains a substantial gap between the number of compounds discovered and those that progress
57 toward clinical development, with advancing candidates often occupying a relatively constrained region of
58 chemical space. A significant reason for this attrition is toxicity; many promising compounds are triaged or
59 exit development early due to a narrow therapeutic index - the difference between the effective
60 therapeutic dose and the dose that causes substantial damage to healthy tissues. Severe toxicities that
61 may be tolerated in other disease indications, such as myelosuppression (16), neuropathy (17), or
62 secondary malignancies (18) are unacceptable for patients with acute infections, who are frequently
63 otherwise healthy. As a result, large portions of the chemical landscape remain underutilized for antibiotic
64 use. Strategies that directly mitigate toxicity therefore represent a powerful opportunity to expand the pool
65 of chemistries accessible for antimicrobial development, enabling the rapid generation of new, structurally
66 diverse antibiotics that carry reduced susceptibility to cross-resistance.

67 In this study, we present a two-armed, generalizable strategy to widen the therapeutic index of
68 toxic compounds and enable their use as antibiotics. As a proof-of-concept, we apply this strategy to
69 calicheamicin, a potent DNA-damaging agent that is approved for cancer treatment, but which causes
70 significant hepatotoxicity that would preclude administration to patients with infections (*4*, *5*). In the first
71 arm of our approach, we formulate calicheamicin as a conditionally-active conjugate, inspired by design
72 principles that have been used to deliver potent cytotoxic payloads in oncology (17,18). In this format, we
73 tether calicheamicin to a carrier protein through a protease-cleavable linker. While conjugated, the
74 cytotoxic activity of calicheamicin is masked until an infection-associated protease releases the drug,
75 thereby confining activity to infected tissue and reducing toxicity to healthy cells, widening the therapeutic
76 index (Fig. 1B). Recognizing that even limited exposure of uninfected tissue to a compound as potent as
77 calicheamicin can cause severe damage, we introduced a second arm into our strategy to neutralize any
78 released, unconjugated drug that travels beyond the infection site**.** To this end, we adapted a natural
79 microbial strategy by harnessing the self-resistance mechanism of *Micromonospora echinospora,* the
80 natural producer of calicheamicin*. M. echinospora* produces several enzymes that neutralize
81 calicheamicin to protect itself from autotoxicity (*6*, *7*); we hypothesized that we could re-engineer and
82 administer these enzymes as “antidotes” to neutralize off-target calicheamicin, further widening the

83 therapeutic index (Fig. 1C). We first show that our calicheamicin-containing drug conjugate exhibits
84 activity dependent on an infection-associated protease against Gram-negative and -positive priority
85 pathogens, and that prior to cleavage, this conjugated format masks calicheamicin toxicity to mammalian
86 cells. We further show that bacterial-derived calicheamicin self-resistance enzymes can be re-engineered
87 to act as long-circulating antidotes that neutralize off-target calicheamicin *in vitro* and *in vivo*, reducing
88 liver toxicity. Finally, we validated that the combination of these two strategies achieves therapeutic
89 efficacy in mouse models of Gram positive and negative bacterial pneumonia, while minimizing systemic
90 toxicity. Together, these results establish a generalizable framework for engineering drug safety and
91 mobilizing potent but toxicity-limited compounds as antimicrobials.

92 **RESULTS**

93 **Calicheamicin has broad spectrum activity against Gram-positive and Gram-negative pathogens**

94 We first evaluated the antimicrobial activity of calicheamicin against a panel of Gram-negative
95 and Gram-positive bacterial pathogens, including several designated as priority pathogens by the World
96 Health Organization (*8*). Measuring microbial susceptibility to calicheamicin using broth microdilution
97 assays, we determined the minimum inhibitory concentration (MIC) of calicheamicin across representative
98 strains (Table 1). We found that calicheamicin had potent activity against the Gram-positive
99 bacterium *Staphylococcus aureus*, with an MIC of 0.0006 μg/mL, a potency that was comparable to or
100 greater than that of a clinically used antibiotic vancomycin (Table 1). Notably, this potency was
101 maintained against a methicillin-resistant *S. aureus* (MRSA) isolate, BA1556. Calicheamicin also
102 demonstrated activity against Gram-negative pathogens including *Pseudomonas aeruginosa*, *Escherichia*
103 *coli*, and *Klebsiella pneumoniae*, with MIC values ranging from 0.015 to 0.5 μg/mL (Table 1). Together,
104 these data demonstrate that calicheamicin exhibits broad-spectrum antimicrobial activity, with efficacy
105 extending to multidrug-resistant strains, and at concentrations that would be realistic for clinical
106 translation.

107 **Conditionally-active drug conjugate masks cytotoxicity while retaining antibacterial activity *in***
108 ***vitro***

109 While the potent antimicrobial activity of calicheamicin is a promising starting point, its substantial
110 toxicity toward mammalian cells, particularly liver cells, precludes its use as a free compound. In
111 oncology, this limitation has been addressed by formulating calicheamicin as an antibody–drug conjugate
112 (*9*, *10*), where targeting and conditional activity improve the therapeutic index. Building on this approach,
113 we developed a conditionally-active calicheamicin conjugate tailored for the infection context. In this
114 design, calicheamicin was tethered to an albumin-binding domain (ABD) via a protease-sensitive linker
115 that masks its cytotoxic activity until cleavage by infection-associated proteases (Fig. 2A). Use of albumin
116 as the carrier protein leverages endogenous trafficking pathways to enhance accumulation (*11*, *12*) ,
117 retention (*13*), and mucopenetration (*14*) at sites of infection. As a linker between albumin and the drug,
118 we used a peptide sequence cleavable by neutrophil elastase, which is enriched at sites of bacterial
119 infection due to immune cell recruitment.

120 To generate the ABD–calicheamicin conjugate (ABD-Cal), we prepared a calicheamicin–peptide
121 intermediate and coupled it to a recombinantly-expressed ABD using strain-promoted azide–alkyne
122 cycloaddition. We next tested whether conjugation masked the cytotoxic activity of calicheamicin and
123 allowed for protease-dependent activation by assessing antibacterial activity and mammalian cell toxicity
124 in the presence or absence of neutrophil elastase *in vitro*. The conjugate was incubated with neutrophil
125 elastase or vehicle control for 4 hours prior to evaluation. We then measured antibacterial activity against
126 a representative Gram-positive (*S. aureus*) (Fig. 2B) and Gram-negative (*K. pneumoniae*) pathogen (Fig.
127 2C). In the absence of protease, we observed no antimicrobial activity; in the presence of protease, we
128 observed a recovery in antimicrobial activity with a (~60-120-fold) change in the minimum inhibitory
129 concentration (MIC) between the intact and cleaved conjugates, depending on the pathogen tested. We
130 also assessed whether formulation of calicheamicin as a conditionally-active conjugate protected
131 mammalian cells from toxicity. We found that in the absence of protease, the intact conjugate
132 demonstrated minimal mammalian toxicity to HepG2 liver cells after 24 hours of exposure (Fig. 2D).
133 Together, these data show that calicheamicin, when formulated as a conditional conjugate, exhibits
134 reduced toxicity toward mammalian cells while conjugated, but regains potent antibacterial activity once
135 released by protease cleavage.

136 **Conditionally-active drug conjugate demonstrates improved safety relative to free drug *in vivo***

137 Having shown *in vitro* that conjugation masks calicheamicin's cytotoxicity and that protease
138 cleavage restores antibacterial activity, we next asked whether restricting activation to the infection
139 microenvironment reduces systemic, particularly hepatic, toxicity *in vivo*. To test this, we compared the
140 liver toxicity of the conditionally active calicheamicin conjugate with free calicheamicin *in vivo*. Healthy
141 mice were intravenously administered either free calicheamicin or the conjugate (dose matched by drug
142 concentration) (Fig. 2E). Liver injury was assessed 36 h post-injection by measuring serum aspartate
143 aminotransferase (AST) levels (Fig. 2F), alanine aminotransferase (ALT) (Fig. 2G) and by histological
144 analysis (Fig. S1). Mice treated with free calicheamicin exhibited elevated AST (Fig. 2F) and ALT (Fig.
145 2G) levels. Mice receiving the conjugate showed a significant reduction in toxicity relative to free drug,
146 although serum liver enzymes were significantly elevated above the baseline of mice treated with vehicle
147 alone. Histology revealed moderate to severe injury in mice treated with free drug, evidenced by diffuse
148 presence of hepatocytes with swollen cytoplasm or shrunken, hypereosinophilic cells (Fig. S1) The livers
149 of conjugate-treated mice showed more mild changes, including some apoptotic cells with swollen
150 cytoplasm, and some healthy cells, consistent with more limited toxicity (Fig. S1). These findings indicate
151 that formulation of calicheamicin as the conditionally-active conjugate significantly reduces off-target
152 hepatotoxicity *in vivo.*

153 **Microbial-derived antidotes can neutralize drug toxicity *in vitro* and *in vivo***

154 Formulation of calicheamicin as a conditional conjugate significantly reduced hepatotoxicity in
155 healthy mice but did not eliminate liver injury, which we hypothesized arose from a fraction of drug
156 released outside the infection site, potentially via low levels of protease-mediated activation outside the
157 infection environment, or diffusion of released drug from infected tissue back into the bloodstream. We
158 therefore developed a second complementary strategy to address these residual sources of toxicity and
159 further improve the safety profile of calicheamicin. To achieve a second layer of toxicity mitigation, we
160 drew inspiration from the natural self-resistance mechanism of *Micromonospora echinospora*, the native
161 producer of calicheamicin, which avoids self-toxicity by enzymatically inactivating the compound. We

162 envisioned adapting this self-resistance strategy for therapeutic use by engineering long-circulating
163 variants of these calicheamicin-neutralizing enzymes to act as “antidotes”, intercepting and neutralizing
164 calicheamicin that escapes the infection microenvironment before it reaches sensitive tissues (Fig. 3A).

165 We first evaluated which of the native self-resistance enzymes would be most suitable for
166 adaptation as a circulating antidote. The calicheamicin biosynthetic cluster encodes three self-resistance
167 enzymes, CalC, CalU16, and CalU19 (*6*, *7*). Reduction of calicheamicin’s trisulfide bond generates the
168 reactive species responsible for its cytotoxicity. CalC and CalU16 act only on this reduced form, whereas
169 CalU19 also neutralizes the unreduced molecule, making it best suited for calicheamicin neutralization in
170 circulation, which is not a reducing environment. We recombinantly expressed CalU19 and sought to
171 confirm its neutralizing activity *in vitro,* by evaluating if administration of CalU19 could protect mammalian
172 cells from calicheamicin-induced toxicity. HepG2 cells were incubated with serial dilutions of
173 calicheamicin in the presence or absence of a fixed concentration of CalU19 for 24 hours, and cell
174 viability was assessed by MTS assay (Fig. 3B). CalU19 conferred protection, with the highest protection
175 observed at lower calicheamicin concentrations, consistent with the stoichiometric mechanism of
176 inactivation in which one molecule of CalU19 is consumed per molecule of calicheamicin neutralized (Fig.
177 3B).

178 Following *in vitro* validation of CalU19 activity, we next assessed its ability to selectively
179 neutralize free calicheamicin without affecting the conjugated drug. During calicheamicin neutralization,
180 CalU19 undergoes a unique self-cleavage event, which can be used as an indicator of neutralizing
181 activity. SDS-PAGE of CalU19 incubated with calicheamicin, ABD-Cal or vehicle, revealed CalU19 self-
182 cleavage fragments only when CalU19 was incubated with free calicheamicin (Fig. S2), confirming that
183 neutralizing activity is restricted to free drug.

184 To realize our design goal of a long-circulating antidote capable of soaking up off-target drug *in*
185 *vivo*, we next engineered CalU19x for *in vivo* administration. We first removed two unpaired cysteines,
186 which could promote off-target interactions with other proteins in vivo, substituting them with alanine to
187 generate CalU19x, which retained neutralizing activity comparable to the wild-type enzyme (Fig. 3B). We

188 then assessed CalU19 *pharmacokinetics in vivo* (Fig. 3C, D). Fluorophore-labeled CalU19 and CalU19x
189 were both rapidly cleared from circulation, with plasma half-lives of ~1 h. To extend the circulation half-life
190 of CalU19x, we generated fusions to single (C-CalU19x) and tandem (LC-CalU19x) albumin-binding
191 domains, as these extend half-life through association with serum albumin. LC-CalU19x exhibited the
192 longest half-life, remaining detectable for at least 48 h in plasma (Fig. 3D), and maintained neutralizing
193 activity *in vitro* comparable to wild-type CalU19 (Fig. 3B).

194 Having established a long-circulating antidote *in vitro*, we next evaluated whether LC-CalU19x
195 could protect against calicheamicin toxicity *in vivo*. Healthy animals were intravenously administered LC-
196 CalU19x or vehicle followed by dosing with calicheamicin (Fig. 3E). Serum and tissue were collected 36-
197 48 h later, and serum AST and ALT levels were quantified. Mice administered calicheamicin and LC-
198 CalU19x showed significantly reduced serum AST (Fig. 3F) and ALT (Fig. 3G) compared with mice
199 administered calicheamicin and vehicle, indicating mitigation of calicheamicin-induced hepatotoxicity.
200 Histology (Fig. S3) agreed with these findings: livers from mice administered calicheamicin and LC-
201 CalU19x-treated mice were largely indistinguishable from healthy controls, whereas mice treated with
202 calicheamicin alone displayed hepatocellular degeneration and necrosis, indicated by swollen cells with
203 eosinophilic cytoplasm (Fig. S3). Together, these results demonstrate that LC-CalU19x acts as a
204 circulating antidote that mitigates off-target toxicity without interfering with the activity of the conditionally-
205 active calicheamicin conjugate, supporting their use as a combined therapy.

206 **Drug conjugate and antidote combination achieves antimicrobial efficacy in mouse models of**
207 **pneumonia**

208 We next evaluated the preclinical potential of the ABD-calicheamicin conjugate and LC-CalU19x
209 in combination, testing whether co-administration of the antidote with the conditionally-active drug could
210 reduce bacterial burden while minimizing liver toxicity in a mouse models of bacterial pneumonia. Mice
211 were infected with *S. aureus*, followed by intratracheal administration of vehicle, ABD-calicheamicin
212 alone, ABD-calicheamicin in combination with intravenously administered LC-CalU19x (Fig. 4A–B), or
213 intravenously administered vancomycin. Treatment of *S. aureus*-infected mice with the conditionally-

active conjugate with or without antidote resulted in a 4-log reduction in lung bacterial burden 6 h compared with the vehicle control, demonstrating that on-target antimicrobial efficacy is preserved in the presence of the antidote (Fig. 4B). At the same timepoint, treatment with vancomycin produced a 1–2-log reduction in bacterial burden (Fig. 4B). To assess safety, we compared liver toxicity between mice treated with ABD-Cal alone or ABD-Cal with LC-CalU19x. We observed a significant reduction in toxicity in mice receiving the conjugate plus antidote relative to the conjugate-only and vehicle groups, as measured by serum AST (Fig. 4C) and ALT (Fig. 4D), with enzyme levels in antidote-treated mice within the healthy range.

To evaluate the generalizability of this approach across pathogens, we additionally tested the drug conjugate and antidote combination in a mouse model of Gram-negative *Pseudomonas aeruginosa* pneumonia (Fig. 4E). In this model, treatment with the drug conjugate with and without antidote resulted in a 3-log reduction in lung bacterial burden relative to vehicle control at 6 h (Fig. 4F). Consistent with the findings in the *S. aureus* model, co-administration of the antidote significantly reduced liver toxicity compared with treatment with conjugate alone, as measured by serum AST and ALT (Fig. 4G–H). Together, these findings demonstrate that pairing a conditionally-active drug conjugate with a long-circulating antidote preserves potent antimicrobial efficacy while substantially reducing systemic toxicity. Furthermore, the conditional drug–antidote strategy is effective across both Gram-positive and Gram-negative pathogens, supporting the potential broad applicability of this platform for the treatment of bacterial infections.

DISCUSSION

In this work, we develop a generalizable, two-component strategy designed to widen the therapeutic index of potential antimicrobial compounds whose clinical translation is otherwise limited by toxicity. Using calicheamicin, a cytotoxin with antimicrobial activity but unacceptable hepatotoxicity, as a proof of concept, we demonstrate that antibacterial activity and host toxicity can be decoupled through the combined use of conditional drug activation to restrict drug activity to infected tissue and active detoxification of off-target drug. Together, this approach enabled therapeutic efficacy in a mouse model of bacterial pneumonia while minimizing hepatotoxicity.

241 Conditional drug conjugates hold considerable potential for infectious disease, but their
242 development in that context is far less common than in oncology, where antibody–drug conjugates
243 (ADCs) have achieved notable clinical success (*11*, *12*, *15*, *16*). The distinct biological context of bacterial
244 infections requires revising design criteria that have guided drug conjugate development in oncology.
245 While oncology relies on antibodies to direct cytotoxic payloads to defined tumor antigens, infection-
246 focused conjugates would benefit from carrier proteins that target the site of infection in an antigen-
247 independent manner and are thus compatible with broad-spectrum activity against a variety of pathogens.
248 Our design (Fig. 2) uses an albumin-binding domain (ABD) as the drug carrier, with the intent to promote
249 retention (*13*) and mucopenetration (*14*) at the sites of infection when administered into the lung. For the
250 linker connecting the carrier protein to the drug, design requirements differ substantially between cancer
251 and bacterial infection. ADCs for cancer typically exploit tumor-associated proteases such as cathepsins
252 to release payloads intracellularly within lysosomes, a defined environment with acidic pH, reducing
253 conditions, and a well-characterized protease repertoire (*17*). In contrast, bacterial infection is likely to
254 require extracellular drug release, which is a heterogeneous environment, where disease-associated
255 triggers act amid variable pH and redox states in the presence of immune cells and cellular debris. To
256 achieve robust and selective activation in such a setting, we incorporated a peptide linker cleavable by
257 neutrophil elastase, which is enriched extracellularly at sites of bacterial infection after release by
258 recruited immune cells (*13*).

259 Formulation of calicheamicin as a conditionally-active conjugate reduced liver toxicity but did not
260 fully eliminate it (Fig. 2), consistent with both preclinical and clinical data from oncology, the context in
261 which conditional-drug conjugates have advanced the furthest clinically. In particular, published evidence
262 suggests that the maximum tolerated doses of some ADCs approach those of the unconjugated payload
263 (*5*, *18*–*20*). Prior efforts have focused on refining aspects of the antibody, linker, or payload to reduce
264 toxicity, but off-target damage in the liver, bone marrow, and gastrointestinal tract remains a major barrier.
265 To move beyond these limitations in the context of infection, we turned to microbes themselves, which not
266 only produce some of the natural products we used as therapeutics, but also encode self-resistance
267 enzymes to protect against autotoxicity. Inspired by this microbial strategy, we introduced a second layer
268 of protection: delivery of an engineered self-resistance enzyme derived from *Micromonospora*

269 *echinospora*, the natural producer of calicheamicin, as an antidote to neutralize circulating free drug
270 outside the site of infection (Fig. 3). While coadministration of antibiotics with compounds that enhance
271 antimicrobial activity are under development (*21–24*), coadministration of agents specifically designed to
272 improve therapeutic safety is less explored in infectious disease. Related coadministration strategies
273 aimed at improving therapeutic safety have begun to be explored in oncology contexts, for example in
274 preclinical work examining neutralization of toxicity for radiation (*25*), and clinically in the administration of
275 agents (*26*) to mitigate cytokine release syndrome after administration of CAR-T therapy.

276 Despite the promise of our drug conjugate and antidote platform, several challenges remain
277 before its translation to clinical settings. Microbial-derived proteins like the antidote we developed may be
278 immunogenic upon repeated administration, as is often required in the treatment of bacterial infections.
279 Existing molecular engineering strategies such as PEGylation (*27*), domain humanization (*28*), or epitope
280 masking (*29*) of the antidote could reduce its immunogenic potential, and there are encouraging
281 examples of regulator-approved and clinically-used products derived from microbial enzymes (*30*, *31*).
282 Second, the success of this dual system hinges on spatial, kinetic, or temporal separation between on-
283 target activity and off-target detoxification. In our current model, we achieve this distinction using physical
284 compartmentalization, via local pulmonary delivery of the drug conjugate and systemic administration of
285 the antidote (Fig 4). This separation between localized activity and off-target neutralization is also
286 achieved by virtue of the conjugate, which protects the conjugated drug from premature deactivation by
287 the antidote, as the enzyme can only bind and neutralize the released, active form of the drug (Fig. S2).
288 However, extending the paired conjugate-antidote system to other sites of infection will require context-
289 specific tailoring. For example, we hypothesize that treatment of systemic bloodstream infections would
290 likely require prophylactic delivery of CalU19, either as a protein or mRNA encapsulated in lipid
291 nanoparticles, such that they can be taken up by liver sinusoidal endothelial cells or hepatocytes to
292 protect these tissues prior to systemic administration and release of calicheamicin from the conjugate in
293 response to cues from the bloodstream infection. The modularity of our platform, with the ability to
294 exchange the carrier protein and protease-susceptible linker components of the conjugate, as well as the
295 possibility of fusing other targeting partners to CalU19 to control half-life or localization within the body,
296 makes such adaptation feasible. Finally, the kinetics of enzyme-mediated neutralization of “off target”

297 drug relative to bacterial uptake and killing by “on target” drug remain incompletely understood. Future
298 studies may benefit from structure-guided engineering or directed evolution of CalU19 to modulate its
299 catalytic efficiency to further enhance the therapeutic window of the conjugate and antidote pair.

300 Beyond calicheamicin, we propose that this dual strategy—(1) formulating drugs as conjugates to
301 achieve selective activity at the site of infection and (2) pairing them with microbial resistance enzymes
302 that neutralize off-target toxicity—represents a generalizable approach for mobilizing antimicrobial
303 compounds whose development or use is limited by toxicity, such as existing antibiotics with narrow
304 therapeutic windows, investigational compounds previously abandoned because of safety or
305 pharmacokinetic liabilities, and newly discovered molecules emerging from genome-mining or machine-
306 learning–driven discovery pipelines(*32*–*35*). Drug conjugates are modular: infection-targeting carrier
307 proteins, conditional linkers, and payloads can be interchanged to suit different pathogens and infection
308 contexts(*36*). Further, microbial resistance mechanisms provide a large reservoir of potential antidotes.
309 Many natural product biosynthetic gene clusters encode self-resistance genes that protect the producing
310 organism from autotoxicity(*37*); related resistance determinants can also be found in organisms within the
311 same ecological communities as natural product producers (*38*) . These genes encode enzymes that can
312 chemically modify, degrade, or sequester a compound, detoxification mechanisms that could be
313 repurposed therapeutically. Advances in genome mining and machine learning could accelerate the
314 discovery and prioritization of additional drug–antidote pairs. Beyond mining natural mechanisms, these
315 same tools may also enable the de novo design of antidotes (*39*, *40*), providing additional routes to
316 engineer safety for antimicrobial compounds.

317 .More broadly, the combined use of the drug conjugate and antidote represents a conceptual shift
318 in antibiotic treatment—towards a form of molecular stewardship—in which each molecule of the
319 antimicrobial is accounted for, with on-target drug directed precisely to the site of infection while off-target
320 drug is actively neutralized. Although mitigation of liver toxicity was a primary goal of this work, the same
321 principle could reduce collateral damage to tissues that are commonly sensitive to cytotoxic agents, such
322 as the bone marrow. Antibiotic-induced dysbiosis of the gut microbiome is another major concern;
323 antibiotic treatment is frequently associated with shifts in microbial composition, overgrowth of

opportunistic pathogens such as *Clostridioides difficile*, and impaired gut barrier function (*41*, *42*). We hypothesize that co-administration of an antidote could attenuate antibiotic-associated microbiome disruption by neutralizing drug before it reaches the gastrointestinal tract. Beyond the host, excreted antibiotics that enter into the environment through sewage and wastewater exert selective pressure on environmental bacteria, which can drive the emergence of resistance through exposure to sublethal concentrations (*43*). The excretion of highly potent cytotoxic compounds such as calicheamicin also raises concerns about ecological toxicity (*44–46*). Incorporation of antidotes into therapeutic regimens may therefore not only improve safety within the patient but also mitigate the broader ecological consequences of antimicrobial use. Finally, outside of the context of infectious disease, we envision antidotes as an enabling technology for conditionally-active conjugates more generally, with the potential to mitigate toxicity in oncology and other therapeutic indications where drugs with potentially severe side effects and dose limiting toxicities are administered.

ACKNOWLEDGEMENTS, FUNDING AND COMPETING INTERESTS

We are grateful to Dr. Laura Kiessling and Dr. Deborah Hung for their scientific insight and support over the course of the work. We are grateful to the Koch Institute Swanson Biotechnology Center, specifically the Histology core (Kathy Cormier, Magalie Boucher) and the Biopolymer and Proteomics core (Heather Amoroso). We are grateful to Kasturi Chakraborthy, Susanna Elledge and Vardhman Kumar for feedback on the manuscript. This work was supported by R01 AI132413 and U19 AI142780 grants from the National Institute of Allergy and Infectious Diseases. This study was supported in part by the Virginia and D.K. Ludwig Fund for Cancer Research, the Koch Institute Support Grant P30-CA14051 from the National Cancer Institute (Swanson Biotechnology Center) and Core Center Grant P30-ES002109 from the National Institute of Environmental Health Sciences. Additional support was received from the Koch Institute's Marble Center for Cancer Nanomedicine. This research was supported in part by a generous gift from Joel Gantcher. T.S. was supported by a postdoctoral fellowship from the Ludwig Center at MIT's Koch Institute for Integrative Cancer Research. S.N.B. is a Howard Hughes Institute Investigator. Competing interests: S.N.B. reports consulting roles and/or equity in Amplifyer Bio, Catalio Capital, Danaher, Earli Inc., Impilo Therapeutics, Matrisome Bio, Ochre Bio, Port Therapeutics, Satellite Bio, Sunbird Bio, and Xilio Therapeutics, which were not involved in this study.

352

353 **MATERIALS and METHODS**

354 **Bacterial strains and culture**

355 *Escherichia coli* ATCC 29522, *Klebsiella pneumoniae* ATCC 43816, *Pseudomonas*
356 *aeruginosa* PAO1, *Staphylococcus aureus* 502A, and *Staphylococcus aureus* USA300_FPR3757 were
357 used in this study. Strains were obtained from the American Type Culture Collection (ATCC) or as
358 indicated. Bacteria were cultured in Mueller–Hinton broth (MHB; BD Difco) at 37 °C with shaking at
359 250 r.p.m. Growth was monitored by optical density at 600 nm (OD600).

360 **Molecular cloning**

361 gBlock™ gene fragments encoding ABD with a C-terminal cysteine ($(ABD)_2$-$(EEG)_6$-Cys), CalC, and
362 CalU19 with flanking restriction sites NcoI and XhoI were ordered from Integrated DNA Technologies,
363 cloned into pET28(a) by restriction enzyme digestion and ligation, and transformed into *E. coli* DH5α
364 competent cells (New England Biolabs). Colonies encoding the correct inserts were confirmed by Sanger
365 sequencing (QuintaraBio), and plasmids were purified using a plasmid miniprep kit (Thermo Fisher
366 Scientific). For CalU19 variants, clonal genes were directly obtained from Twist Bioscience already cloned
367 into the pET28(a) expression vector. All expression plasmids were subsequently transformed into *E. coli*
368 BL21(DE3) cells for protein expression.

369

370 **Protein expression**

371 A secondary culture (500 mL LB broth (50 µg/mL kanamycin)) of *E coli.* BL21(DE3) encoding the protein of
372 interest was expanded from an overnight primary culture (3 mL) in an incubator shaker at 37 °C until OD600
373 reached about 0.6 (~ 4hours). Protein expression was induced by addition of an IPTG solution to a final
374 concentration of 1 mM. The induced culture was incubated in an incubator shaker for 2 h at 37 °C after
375 which the culture was centrifuged and the bacteria pellet was frozen and stored in a -80 °C freezer. For
376 purification, the bacteria pellet was thawed in a 37 °C water bath and lysed with a B-PER™ complete
377 bacterial protein extraction reagent (ThermoFisher). The lysed solution was centrifuged and the
378 supernatant was incubated with Qiagen Ni-NTA agarose for 30minutes at 4 °C to capture the product. The

379 agarose was transferred to a fritted column, washed sequentially with a wash buffer A (50 mM Tris, 500
380 mM NaCl, 2% Triton X-114) (10 column volumes (CVs)) and a wash buffer B (50 mM Tris, 500 mM NaCl)
381 (10 column volumes) before elution with an elution buffer (500 mM imidazole, 50 mM Tris, 500 mM NaCl,
382 10% glycerol) (3 CVs). The purified protein was confirmed via SDS-PAGE analysis with Coomassie blue
383 staining.
384

385 **Synthesis of Conjugate Azide-AAPV-calicheamicin**

386 An N-terminal azidoacetylated peptide substrate with a C-terminal penicillamine (Pen) (Azide-AAPV-Pen)
387 was synthesized by CPC Scientific via a standard Fmoc-based solid phase peptide synthesis. A solution of
388 calicheamicin (1 eq.) (MedChemExpress) in N,N-dimethylformamide (DMF) was added to a solution of
389 Azide-AAPV-Pen (3 eq.) in DMF followed by addition of triethylamine (8 eq.) to the reaction solution. The
390 reaction solution was purged with nitrogen for 5minutes and incubated for 24hours at 4 °C. The Azide-
391 AAPV-calicheamicin product was purified by the Koch Institute Biopolymers & Proteomics core facility using
392 a semi-preparative HPLC column and confirmed with MALDI-ToF MS.
393 $(ABD)_2$-$(EEG)_6$-Cys was incubated with TCEP (10 eq.) for 30minutes at RT and buffer-exchanged into PBS
394 (1 mM EDTA, pH 6.5) using an Amicon 10-kDa, ultra-0.5 centrifugal filter unit (14,000 rpm, 2minutes, 4
395 times). The reduced protein was incubated with DBCO-Maleimide (4 eq.) for 4hours at RT. The ABD-DBCO
396 product was purified and buffer-exchanged into PBS using a PD-10 desalting column (Cytiva).
397 *Synthesis of ABD-calicheamicin conjugates*
398 Azide-Sx-calicheamicin (2 eq.) was dissolved in DMF and added to a solution of ABD-DBCO (1 eq.) in PBS
399 to a final concentration of 50% DMF. The reaction solution was incubated for 24hours at RT and centrifuged
400 to remove precipitate. The product in supernatant was immobilized on Ni-NTA agarose, washed with a
401 wash buffer C (50 mM Tris, 500 mM NaCl, 20% DMF) (10 CVs) and a wash buffer B (10 CVs) before elution
402 with the elution buffer. The product was buffer-exchanged into PBS using a PD-10 desalting column and
403 quantified via absorbance at 200 nm. The product was confirmed and assessed for percentage purity using
404 SDS-PAGE analysis.

405 ***In vitro* activity and toxicity masking**

406 To evaluate conditional activation, ABD–calicheamicin conjugates were incubated with recombinant
407 human neutrophil elastase (Enzo Life Sciences) or vehicle control in PBS at 37 °C for 4 h. Reaction
408 mixtures were then diluted into bacterial or mammalian assay media as described below. Minimum
409 inhibitory concentrations (MICs) were determined in accordance with CLSI guidelines. Briefly, bacteria
410 were seeded at OD 0.005 in 96-well plates containing MHB supplemented with conjugate, protease-
411 treated conjugate, or controls. Plates were incubated at 37 °C for 24 h, and bacterial growth was
412 assessed by measuring optical density at 600 nm (SpectraMax i3, Molecular Devices). MICs were defined
413 as the lowest concentration of conjugate preventing visible bacterial growth. Human hepatocellular
414 carcinoma cells (HepG2, ATCC HB-8065) were maintained in Dulbecco's Modified Eagle Medium
415 (DMEM; Thermo Fisher Scientific) supplemented with 10% fetal bovine serum (FBS) and 1% penicillin–
416 streptomycin. For cytotoxicity assays, HepG2 cells were seeded at 1 × 10^4 cells per well in collagen-
417 coated 96-well plates and allowed to adhere overnight. Cells were then exposed to intact or protease-
418 treated ABD–calicheamicin conjugates for 24 h. Viability was quantified using the CellTiter AQueous MTS
419 assay (Promega) according to the manufacturer's instructions, and absorbance was read at 490 nm using
420 a plate reader. In vitro activity and toxicity data were fit using a four-parameter logistic (4PL) sigmoidal
421 model, where X represents concentration, in GraphPad Prism (GraphPad Software).

422 ***In vitro* CalU19 neutralization evaluation**

423 *SDS-PAGE* CalU19 was labeled with Cy7 through random lysine labeling and incubated with vehicle,
424 calicheamicin, or ABD-Cal for 4 hours at 37C. At 4h, reactions were run on a gel (NuPAGE™ 4-12% Bis-
425 Tris Protein Gels, 1.0 mm, 12-well, Thermofisher) which was then imaged using an Odyssey CLx imager
426 in the 800 nm channel, for detection of Cy7 fluorescence, monitoring specifically for the presence of the
427 intact protein at ~27 kDa, as well as the self-cleavage fragments at 6kDa and 21 kDa.

428 *Cytotoxicity Assay* HepG2 cells were seeded at 1 × 10^4 cells per well in collagen-coated 96-well plates
429 and allowed to adhere overnight. Cells were then exposed to serial dilutions of calicheamicin, in the
430 presence of absence of 5 μM CalU19, CalU19x, C-CalU19X, LC-CalU19x, or vehicle (for the control).
431 Viability was quantified at 24 h using the CellTiter AQueous MTS assay (Promega) according to the

432 manufacturer's instructions, and absorbance was read at 490 nm using a plate reader. Data were fit using
433 a four-parameter logistic (4PL) sigmoidal model, where X represents concentration, in GraphPad Prism
434 (GraphPad Software).

435 ***In vivo* pharmacokinetics, activity and toxicity evaluation**

436 All animal studies were approved by the Massachusetts Institute of Technology's Committee on Animal
437 Care (MIT CAC protocol 2203000310). For infected mice, bacterial inoculum was prepared from mid-
438 logarithmic phase cultures grown in Mueller–Hinton broth, washed twice with PBS, and quantified by
439 optical density and serial dilution plating. Following administration, mice were monitored continuously until
440 recovery from anesthesia and then observed at regular intervals for clinical signs of infection, including
441 weight loss, respiratory distress, and reduced activity. For lung infections, CD-1 mice (10-12 weeks old)
442 were administered 1.25 x 10^8 CFU of *S. aureus* (502A) (suspended in PBS) or 5 x 10^6 CFU of *P.*
443 *aeruginosa* (suspended in PBS) by intratracheal administration using a 22G blunt end catheter and
444 monitored after administration. At designated time points post-infection, mice were euthanized, lungs
445 were aseptically harvested, and/or blood was collected.

446 *CFU quantification* Lungs were weighed and homogenized in sterile PBS using gentleMACS M-tubes
447 (Miltenyi Biotec). Homogenates were serially diluted and plated on mannitol salt agar (BD Difco) to
448 selectively recover *S. aureus*, and Pseudomonas Isolation Agar (Sigma-Aldrich) with colonies were
449 enumerated after 24 h incubation at 37 °C. Samples with no detectable colonies on plates were recorded
450 as below the limit of detection. For graphical representation and statistical comparison, these samples
451 were assigned a value equal to the limit of detection.

452 *Histology* Lungs were fixed in 10% neutral buffered formalin for at least 48 h, processed, and paraffin-
453 embedded by the Koch Institute Histology Core Facility. Tissue sections (X µm) were stained with
454 hematoxylin and eosin (H&E) and imaged using brightfield microscopy. Histological evaluation was
455 performed by

456 *Toxicity evaluation* To evaluate liver toxicity, blood was collected from mice at designated time points via
457 terminal cardiac puncture. Whole blood was allowed to clot at room temperature in BD Microtainer SST
458 tubes with gold tops (BD Biosciences, Cat. No. 365967). The resulting serum was aliquoted and stored at
459 –80 °C until analysis. Serum alanine aminotransferase (ALT) activity was quantified using a colorimetric
460 assay kit (Thermo Fisher Scientific, ALT/GPT Activity Assay Kit, Cat. No. EEA001, and serum aspartate
461 aminotransferase (AST) activity was measured using a colorimetric assay kit (MilliporeSigma, AST
462 Activity Assay Kit, Cat. No. MAK055), following the manufacturers' protocols. Absorbance was read using
463 a microplate reader (SpectraMax i3, Molecular Devices).

464 *Pharmacokinetics* CalU19 variants were conjugated with Cy7 through random lysine labeling. Labeled
465 proteins were administered intravenously to CD-1 mice. At the indicated time points, blood was collected
466 from the tail vein using heparinized capillary tubes, diluted in PBS containing EDTA, and centrifuged to
467 remove cells. Fluorescence in plasma supernatants was quantified using a microplate reader to
468 determine circulating protein concentrations. Percentage of antidote protein remaining in circulation was
469 calculated as the percentage of antidote at each timepoint relative to the 1 min timepoint.

470 **Statistical Analysis and Schematic Representation**

471 Statistical analyses were performed with GraphPad Prism. Data are plotted as mean ± SD. Comparisons
472 among different treatment groups are based on one-way ANOVA with Tukey *post hoc* tests. A P value <
473 0.05 was considered statistically significant. Parts of the schematics in this publication were created with
474 BioRender.

475

476 **REFERENCES**

477 1. M. Naghavi *et al.*, *The Lancet*. **404**, 1199–1226 (2024).
478 2. C. Årdal *et al.*, *Nat Rev Microbiol*. **18**, 267–274 (2020).
479 3. F. Ruggieri *et al.*, *European Journal of Medicinal Chemistry*. **256**, 115413 (2023).
480 4. F. J. Giles *et al.*, *Cancer*. **92**, 406–413 (2001).
481 5. M. Guffroy *et al.*, *Clin Cancer Res*. **23**, 1760–1770 (2017).
482 6. J. B. Biggins, K. C. Onwueme, J. S. Thorson, *Science*. **301**, 1537–1541 (2003).

483 7. S. I. Elshahawi *et al.*, *ACS Chem Biol*. **9**, 2347–2358 (2014).

484 8. WHO bacterial priority pathogens list, 2024: Bacterial pathogens of public health importance to
485 guide research, development and strategies to prevent and control antimicrobial resistance,
486 (available at https://www.who.int/publications/i/item/9789240093461).

487 9. E. L. Sievers *et al.*, *Blood*. **93**, 3678–3684 (1999).

488 10. E. L. Sievers *et al.*, *J Clin Oncol*. **19**, 3244–3254 (2001).

489 11. C. Ngambenjawong, L. W. Chan, H. E. Fleming, S. N. Bhatia, *ACS Nano*. **16**, 15779–15791 (2022).

490 12. C. Ngambenjawong *et al.*, *ACS Nano*. **19**, 9958–9970 (2025).

491 13. L. W. Chan *et al.*, *Nat. Nanotechnol.* **15**, 792–800 (2020).

492 14. K. Rakhra *et al.*, *Science Immunology*. **6**, eabd8003 (2021).

493 15. S. M. Lehar *et al.*, *Nature*. **527**, 323–328 (2015).

494 16. K. K. Kajihara *et al.*, *mBio*. **12**, e00202-21.

495 17. J. D. Bargh, A. Isidro-Llobet, J. S. Parker, D. R. Spring, *Chem. Soc. Rev.* **48**, 4361–4374 (2019).

496 18. R. Colombo, J. R. Rich, *Cancer Cell* (2022), doi:10.1016/j.ccell.2022.09.016.

497 19. H.-P. Gerber, S. Gangwar, A. Betts, *MAbs*. **15**, 2230618.

498 20. J. E. Fisher, *Antibodies (Basel)*. **10**, 15 (2021).

499 21. J. Joseph, S. Boby, S. Mooyottu, M. S. Muyyarikkandy, *npj Antimicrob Resist*. **3**, 53 (2025).

500 22. C. Reading, M. Cole, *Antimicrob Agents Chemother*. **11**, 852–857 (1977).

501 23. J. M. Stokes *et al.*, *Nat Microbiol*. **2**, 17028 (2017).

502 24. N. Blondiaux *et al.*, *Science*. **355**, 1206–1211 (2017).

503 25. A. R. Kirtane *et al.*, *Nat. Biomed. Eng*. **9**, 1240–1253 (2025).

504 26. K. Mestermann *et al.*, *Science Translational Medicine*. **11**, eaau5907 (2019).

505 27. J. M. Harris, R. B. Chess, *Nat Rev Drug Discov*. **2**, 214–221 (2003).

506 28. P. J. Carter, A. Rajpal, *Cell*. **185**, 2789–2805 (2022).

507 29. L. V. Zinsli, N. Stierlin, M. J. Loessner, M. Schmelcher, *Comput Struct Biotechnol J*. **19**, 315–329
508 (2021).

509 30. A. E. Place *et al.*, *Lancet Oncol*. **16**, 1677–1690 (2015).

510 31. L. C. Hurst *et al.*, *New England Journal of Medicine*. **361**, 968–979 (2009).

511 32. N. K. Prasad, I. B. Seiple, R. T. Cirz, O. S. Rosenberg, *Antimicrobial Agents and Chemotherapy*. **66**,
512 e00054-22 (2022).

513 33. L. J. V. Piddock, R. Malpani, A. Hennessy, *ACS Infect. Dis.* **10**, 2445–2447 (2024).

514 34. U. Theuretzbacher, K. Outterson, A. Engel, A. Karlén, *Nat Rev Microbiol*. **18**, 275–285 (2020).

515 35. L. L. Silver, *Clin Microbiol Rev*. **24**, 71–109 (2011).

516 36. A. Beck, L. Goetsch, C. Dumontet, N. Corvaïa, *Nat Rev Drug Discov*. **16**, 315–337 (2017).

517 37. X. Chen, H.-X. Pan, G.-L. Tang, *Antibiotics (Basel)*. **12**, 35 (2022).

518 38. J. M. Munita, C. A. Arias, *Microbiology Spectrum*, in press, doi:10.1128/microbiolspec.vmbf-0016-
519 2015.

520 39. P.-S. Huang, S. E. Boyken, D. Baker, *Nature*. **537**, 320–327 (2016).

521 40. A. E. Chu, T. Lu, P.-S. Huang, *Nat Biotechnol*. **42**, 203–215 (2024).

522 41. J. de la Cuesta-Zuluaga, L. Boldt, L. Maier, *Cell Host & Microbe*. **32**, 786–793 (2024).

523 42. B. P. Willing, S. L. Russell, B. B. Finlay, *Nat Rev Microbiol*. **9**, 233–243 (2011).

524 43. D. G. J. Larsson, C.-F. Flach, *Nat Rev Microbiol*. **20**, 257–269 (2022).

525 44. Fate and effects of cytostatic pharmaceuticals in the environment and the identification of
526 biomarkers for and improved risk assessment on environmental exposure | FP7. *CORDIS |*
527 *European Commission*, (available at https://cordis.europa.eu/project/id/265264/reporting).

528 45. A. Castellano-Hinojosa, M. J. Gallardo-Altamirano, J. González-López, A. González-Martínez, *J*
529 *Hazard Mater*. **447**, 130818 (2023).

530 46. S. Mukherjee, D. Mehta, K. Dhangar, M. Kumar, *Chemical Engineering Journal*. **407**, 127184
531 (2021).

532

533

534 **FIGURES AND TABLES**

535

Table 1

	Calicheamicin γ1
Pseudomonas aeruginosa PAO1	0.11 μg/mL (78.1 nM)
Escherichia coli KS1	0.013 μg/mL (9.23 nM)
Klebsiella pneumoniae ATCC43816	0.05 μg/mL (312.5 nM)
Staphylococcus aureus 502A*	0.00061 μg/mL (835 pM)
BA1566 (MRSA)	0.00061 μg/mL (835 pM)

*For comparison, MIC of vancomycin for SA 502A was measured as 1 μg/mL

Table 1 Antibacterial activity of calicheamicin against representative Gram-negative and Gram-positive pathogens.
Minimum inhibitory concentrations (MICs) were determined by microdilution assay in Mueller–Hinton medium supplemented with 3% DMSO. Data represent biological triplicates.

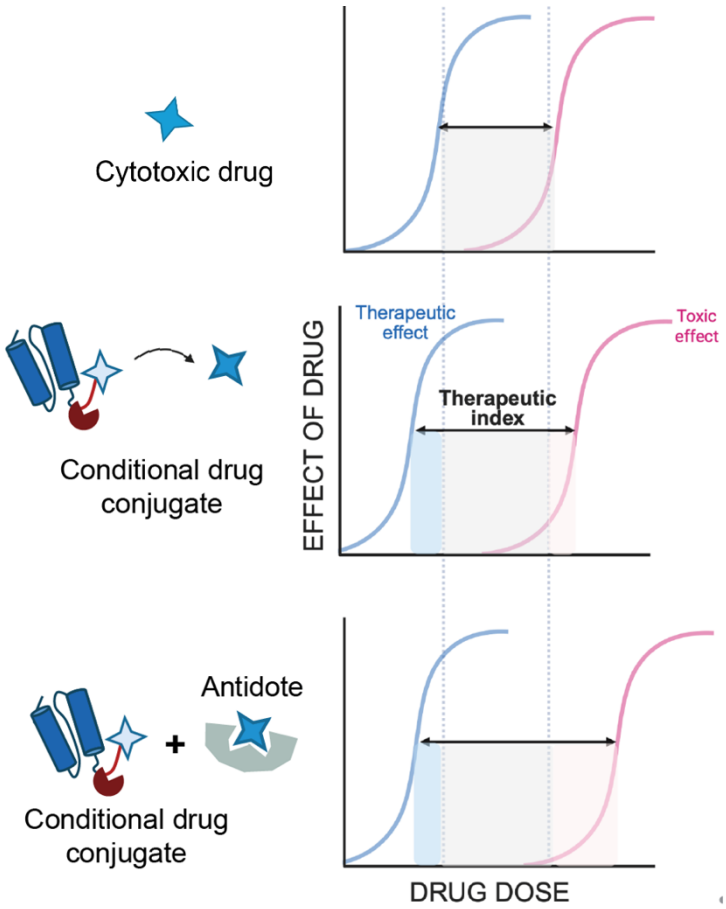

Figure 1. Dual strategy to expand the therapeutic index of toxic compounds for antimicrobial use. (Top) A narrow therapeutic index, defined as the difference between the median therapeutic effect and the median toxic effect, constrains the utility of cytotoxins (blue star) as antimicrobials. (Middle) Formulation of cytotoxins as conditionally active conjugates can widen the therapeutic index by restricting drug activity to an infection site, where proteases (red pac-man) release drug from the conjugate. (Bottom) “Antidotes” derived from self-resistance enzymes further widen the therapeutic index by neutralization off-target drug.

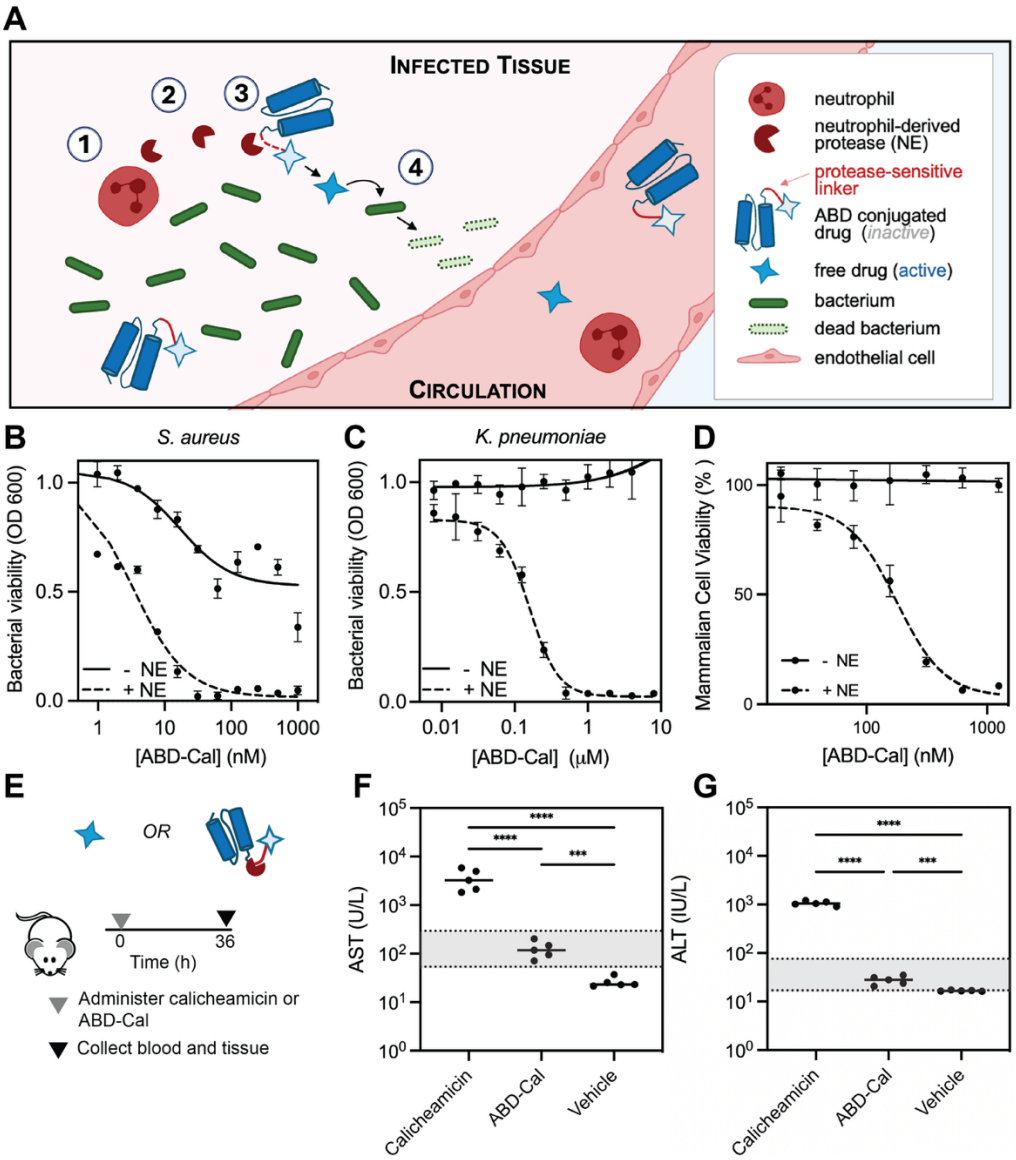

538

Figure 2. ABD-calicheamicin conjugate demonstrates masked mammalian toxicity and protease-triggered antibacterial activity *in vitro* and improved safety *in vivo*. (A) Schematic of ABD-calicheamicin conjugate (ABD-Cal) activation within the infection microenvironment. Within the infection environment, 1) neutrophils are recruited and 2) secrete neutrophil elastase which 3) cleaves and releases calicheamicin from the conjugate 4) such that it can kill bacteria. (B-C) Antimicrobial activity of ABD-Cal evaluated via microdilution assays against representative (B) Gram-positive and (C) Gram-negative bacterial strains in the presence or absence of recombinant neutrophil elastase. Bacterial growth measured by absorbance at 600 nm and normalized to untreated controls. Fold change in antimicrobial activity calculated as the ratio of MIC values of intact vs. cleaved conjugates. (mean ± sd, n = 3 biological replicates) (D) Masked mammalian toxicity of ABD-Cal evaluated via MTS cell proliferation assay in HepG2 cells. Cell viability measured by absorbance at 490 nm and normalized to untreated controls. Fold change in cytotoxicity calculated as the ratio of IC_{50} values of intact vs. cleaved conjugates. (mean ± sd, n = 3 biological replicates) (E) Schematic of experimental timeline of mice administered free calicheamicin (0.025 mg/kg) compared with ABD-Cal (0.025 mg/kg drug eq.) (F) Serum AST and (G) ALT. Dashed lines indicate normal healthy range. (n = 5 biological replicates. Statistical significance was determined by one-way ANOVA followed by Tukey's post hoc test). *P < 0.001* (***); *P* < 0.0001 (****)

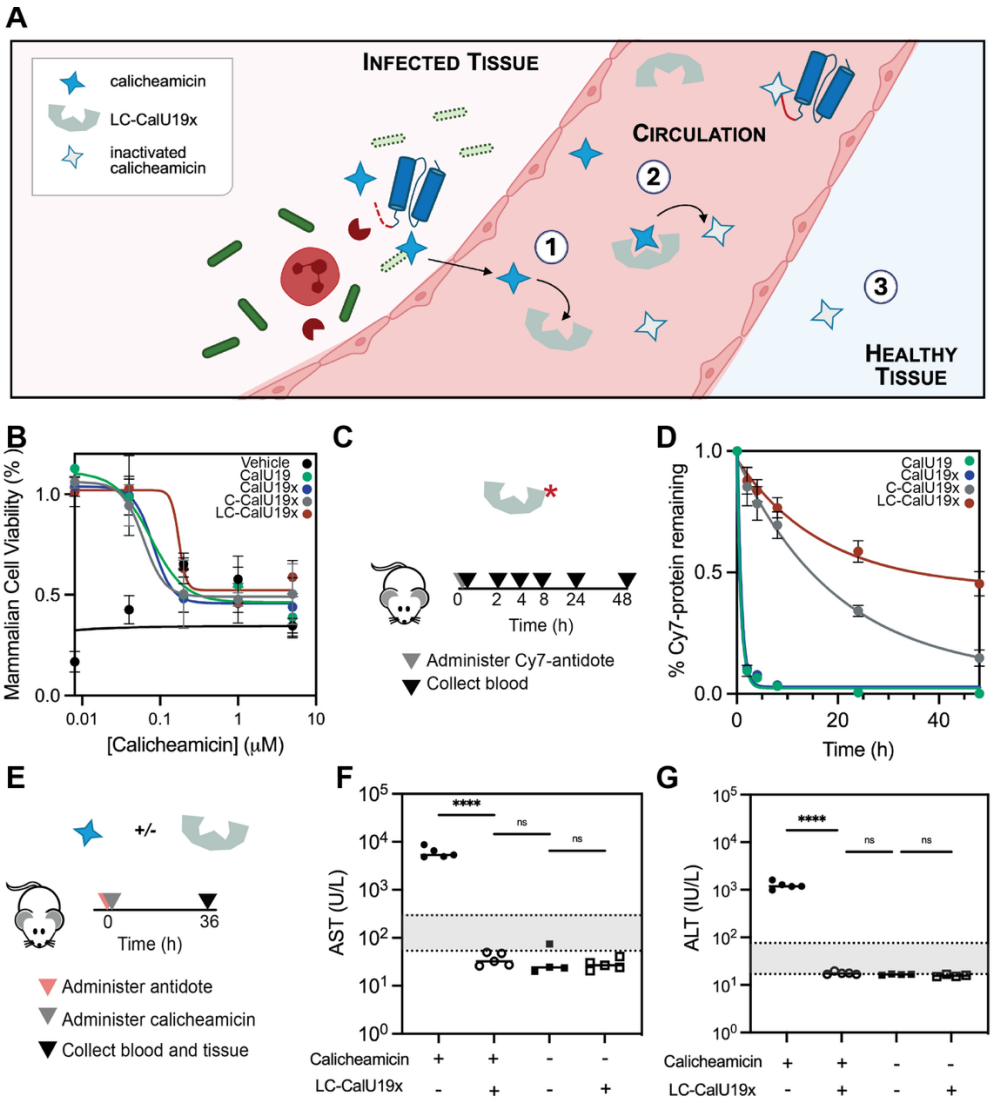

539

Figure 3. Microbial-inspired antidotes protect against calicheamicin-mediated liver toxicity *in vitro* and *in vivo.* Schematic illustrating neutralization of calicheamicin by engineered microbial self-resistance enzymes ("antidotes"). After neutrophil-elastase–mediated cleavage of the ABD–calicheamicin conjugate, either on-target (within the infection microenvironment) or off-target (within healthy tissue) released calicheamicin can 1) enter circulation, where it is 2) bound and inactivated by LC-CalU19x, such that exposure of healthy tissue to active drug is reduced. (B) Calicheamicin neutralization by engineered variants of CalU19 (evaluated via cell proliferation assay in HepG2 cells. Cell viability measured by absorbance at 490 nm and normalized to untreated controls. mean ± sd, n = 4 biological replicates. (C) Schematic of timeline during which Cy7-conjugated proteins were assayed for clearance from plasma. (D) Pharmacokinetics of antidote variants following systemic injection, with plasma concentrations of Cy7 quantified over time. (mean ± sd, n = 4–5 mice per group) (E) Schematic of *in vivo* neutralization of free calicheamicin by LC-CalU19x. (F) Serum AST and (G) ALT levels measured 36 h after calicheamicin administration with or without antidote treatment. Dashed lines indicate normal healthy range (n = 5 Statistical significance determined by one-way ANOVA followed by Tukey's post hoc test.) $P < 0.0001$ (****); ns: not significant.

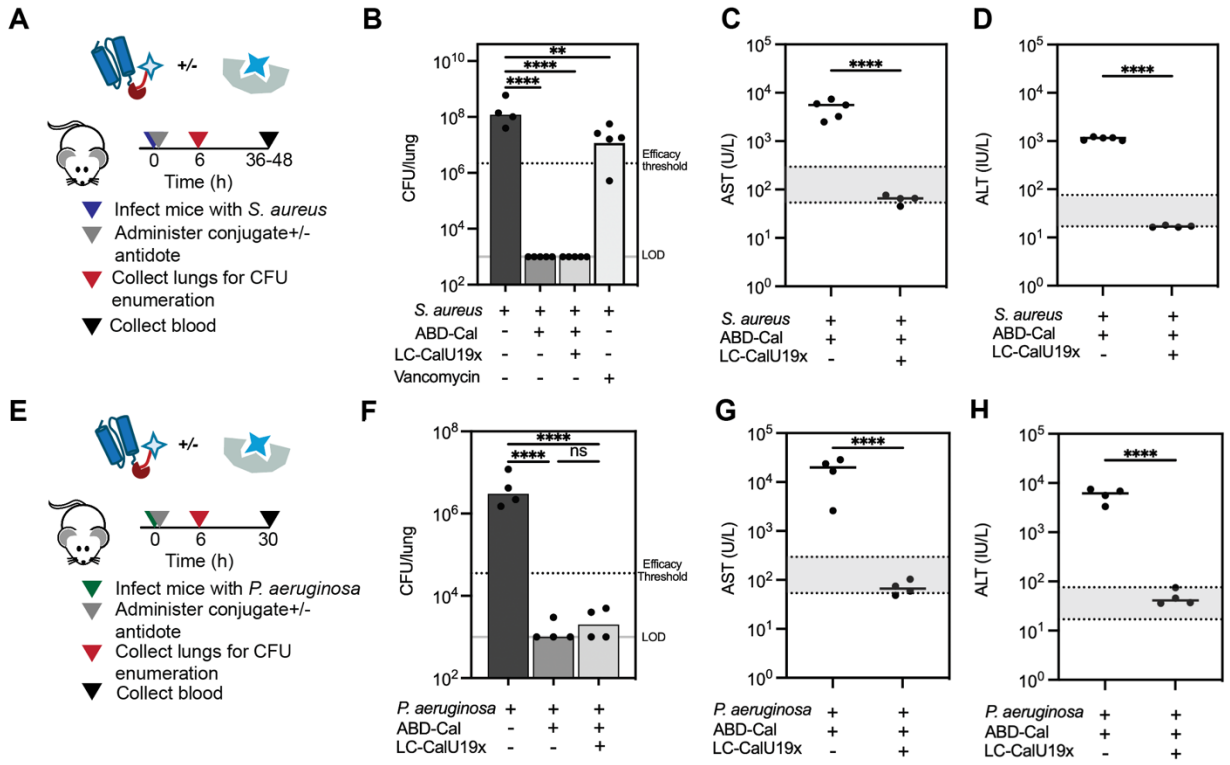

540

Fig. 4 Therapeutic efficacy of calicheamicin conjugate and neutralizing antidote in a murine models of Gram positive and negative bacterial pneumonia. (A) Schematic of experimental timeline for treatment of *S. aureus* pneumonia. For lung bacterial burden and serum chemistry analyses, separate cohorts of animals were used for tissue or blood collection at the indicated time points. (B) Bacterial burden in lungs 6 h post-treatment in mice infected with *Staphylococcus aureus* 502A and treated intratracheally with vehicle, treated intratracheally with calicheamicin drug conjugate (0.25 mg/kg calicheamicin eq) (ABD-Cal) and then intravenously with vehicle or antidote (LC-CalU19x), or treated intravenously with vancomycin (110 mg/kg). Each point represents an individual animal (n = 4-5 per group). Dashed line indicates the threshold for efficacy, defined as a two-log reduction in bacterial burden from the vehicle treated group. Grey line indicates the limit of detection for CFU quantification. Statistical significance determined by one-way ANOVA followed by Dunnett's post hoc test. (C) Serum levels of AST and (D) ALT measured 36-48 h after infection and treatment with ABD-Cal, in the presence or absence of antidote. Each point represents an individual animal (n = 4–5 per group). Dashed lines indicate the normal healthy range. Statistical significance was determined by unpaired t-test. (E) Schematic of experimental timeline for treatment of *P. aeruginosa* pneumonia. (F) Bacterial burden in lungs 6 h post-treatment in mice infected intratracheally with *Pseudomonas aeruginosa* PAO1 and treated intratracheally with vehicle or ABD-Cal (0.4 mg/kg calicheamicin eq) and then intravenously with vehicle or antidote (LC-CalU19x). Each point represents an individual animal (n = 4 per group). Statistical significance determined by one-way ANOVA followed by Tukey's post hoc test. (G) Serum levels of AST and (H) ALT measured 30 h after infection and treatment with ABD-Cal, in the presence or absence of antidote. Each point represents an individual animal (n = 4 per group). Dashed lines indicate the normal healthy range. Statistical significance was determined by unpaired t-test. $P < 0.01$ (**); $P < 0.001$ (***); $P < 0.0001$ (****).

541 **SUPPLEMENTARY FIGURES**

542 Figure S1. H&E-stained liver sections from mice receiving calicheamicin vs. ABD–Cal

543 Figure S2. CalU19 neutralizes free calicheamicin but not ABD-Cal

544 Figure S3. H&E-stained liver sections from mice receiving calicheamicin with or without LC-CalU19x.

545